

Single parameter recovery from modelled
spectra. A comparison of spectral filter
optimisation with standard multivariate
approaches.

Ela Claridge Mark O'Dwyer

March 17, 2005

Abstract

When light is incident on an object it gives rise to a reflectance spectrum which our eyes filter into three colour (red, green and blue) intensities. The novel technique of 'spectral filter optimisation' uses $N+1$ filters to recover N different parameter values which contribute to a given spectrum. The technique chooses filters which, when applied to sample spectra representing all points in N dimensional parameter space, minimize the uncertainty in recovered parameter values. In this report we describe the technique in general and apply it to a simple one-dimensional parameter space problem. In this problem the spectrum of reflected light from a material with known light scattering and absorption characteristics laid on top of a material with similar light interaction behaviour is modelled. The single parameter being studied is the thickness of the top material and the technique finds two filters which, when applied to each spectrum in a set of standard spectra, minimise the errors in estimating the known thicknesses of that set given that each spectrum will have some noise associated with it. We study four cases in which the absorption characteristics of the two materials become increasingly similar and observe the ability of the technique to estimate the unknown top layer thickness from a spectrum with increasing levels of added Gaussian noise. In order to assess the value of the technique we compare results with well known linear multivariate spectral analysis methods. As expected the ability to estimate the top layer thickness is reduced as the standard deviation of added noise is increased and as the two materials' absorption characteristics become more alike but the technique consistently performs better than the linear multivariate methods because of its inherent error handling capability.

Contents

1	Introduction	2
2	Spectral Filter Optimisation	3
2.1	A simple reflectance model	3
2.2	The N+1 filter model	4
2.3	The N+1 filter model when N=1	6
3	Linear Multivariate Techniques	7
4	Experimental method	9
4.1	The one-dimensional problem	9
4.2	The sample reflectance spectra	11
4.3	Results	12
5	Discussion	22

Chapter 1

Introduction

The technique of spectral filter optimisation (SFO) has been developed to enable an accurate assessment of the relative abundance of blood and melanin in the skin when the area of interest is photographed using a digital camera with suitable colour filters[1]. In this report we describe the technique and apply it to a simplified problem (with only one unknown parameter to be determined). As part of the process of SFO it is necessary to produce sample spectra covering the range of interest of the unknown parameter whilst linear multivariate calibration techniques attempt to model the relation between a dependent variable (our parameter of interest) and the measured independent variables (our sample spectra)[2].It is therefore beholden upon us to compare the novel SFO technique with the classical linear multivariate techniques of Principal Component Regression (PCR) and Partial Least Squares (PLS) when applied to our data and to show the relative advantages and disadvantages of the new technique. In particular, when describing SFO, it will become apparent that the technique explicitly incorporates assumptions about the errors involved in physical measurements of data which the linear multivariate methods do not.

Chapter 2

Spectral Filter Optimisation

2.1 A simple reflectance model

When light of a given spectral intensity $I_i(\lambda)$ is incident on the surface of a material some of it will undergo Fresnel interface reflectance (sometimes referred to as spectral or surface reflectance) and the remainder will enter the material where it may be scattered or absorbed. Emerging scattered light (which we shall refer to as body reflectance) will add to the interface reflectance to yield the remitted spectrum $I_r(\lambda)$.

In the dichromatic reflection model of Shafer [3] or the standard reflectance model [4] the spectrum of remitted light intensity, $I_r(\lambda)$, from any point on the surface into a particular direction can be expressed as the sum of a surface reflectance and a body reflectance and each of these can be expressed as the product of a scalar geometry term and a wavelength dependent term which is independent of geometry.

$$I_r(\lambda) = L_s(\lambda)G_s + L_b(\lambda)G_b \quad (2.1)$$

where $L_s(\lambda)$ and $L_b(\lambda)$ are the spectral distributions of the intensities remitted from the surface and body components respectively and G_s and G_b are geometric scale factors. Thus, if the position from which a point on the surface of an object is being observed changes or if the position from which the point on the surface is being illuminated changes then the remitted spectra from surface and body will each have an unchanged wavelength dependent factor whose scaling changes. If we define wavelength reflectance functions $h_s(\lambda)$ and $h_b(\lambda)$ such that $L_s(\lambda) = h_s(\lambda)I_i(\lambda)$ and $L_b(\lambda) = h_b(\lambda)I_i(\lambda)$ we can write

$$I_r(\lambda) = I_i(\lambda)h_s(\lambda)G_s + I_i(\lambda)h_b(\lambda)G_b \quad (2.2)$$

Healey [5] has shown the validity of these approximations when the scattering material is metal (the body scattering term is neglected) and when the scatterer is a dielectric. Lee [6] and Tominaga & Wandell [4] [7] have used the model to separate the interface reflectance from the body reflectance. Preece & Claridge [8], in considering the reflectance from skin, ignore the interface reflectance and derive a technique which enables N parameter recovery using N+1 colour filters to characterise the reflectance spectra.

2.2 The N+1 filter model

Ignoring the interface reflectance term in 2.2 we have

$$I_r(\lambda) = I_i(\lambda)h_b(\lambda)G_b \quad . \quad (2.3)$$

Applying a set of filters $F_l(\lambda)$ $l = 1, 2, \dots, N + 1$ to the reflectance spectrum will yield a set of image values

$$c_l = G_b \int I_i(\lambda) h_b(\lambda) F_l(\lambda) d\lambda \quad l = 1, 2, \dots, N + 1 \quad (2.4)$$

associated with each reflectance spectrum. By constructing the N ratios

$$q_m = \frac{c_{m+1}(\lambda)}{c_1(\lambda)} = \frac{\int I_i(\lambda) h_b(\lambda) F_{m+1}(\lambda) d\lambda}{\int I_i(\lambda) h_b(\lambda) F_1(\lambda) d\lambda} \quad m = 1, 2, \dots, N \quad (2.5)$$

Preece & Claridge [8] created a geometry independent relationship between the object being imaged and the quotients q_m . In addition to removing dependence on the term G_b , the brightness of the illuminant can also be ignored since the incoming intensity can be arbitrarily normalised

$$I_i(\lambda) = \kappa I_{0,i}(\lambda)$$

without affecting equation 2.5.

Consider imaging a scene with N parameters. We define an N dimensional space P (parameter space) in which the vector $\mathbf{p} = \langle p_1, p_2, \dots, p_N \rangle$ (where p_j is the value of parameter j) represents one point. Each such point gives rise to a reflectance spectrum which we derive through a suitable model and then, by a suitable choice of N+1 filters, to the quotient vector $\mathbf{q} = \langle q_1, q_2, \dots, q_N \rangle$ (via equation 2.5) in N dimensional Q space. This defines the vector mapping \mathbf{v} from parameter space to quotient space

$$\mathbf{q} = \mathbf{v}(\mathbf{p})$$

with its associated Jacobian

$$\mathbf{J} = \begin{pmatrix} \frac{\partial q_1}{\partial p_1} & \frac{\partial q_1}{\partial p_2} & \dots & \frac{\partial q_1}{\partial p_N} \\ \dots & \dots & \dots & \dots \\ \frac{\partial q_N}{\partial p_1} & \frac{\partial q_N}{\partial p_2} & \dots & \frac{\partial q_N}{\partial p_N} \end{pmatrix} . \quad (2.6)$$

If the mapping \mathbf{v} is chosen so that the determinant of the Jacobian is non-zero over the whole of parameter space then we can say that the mapping is locally one-to-one and invertible for any value of \mathbf{p} . Thus, at any point in parameter space we can construct the inverse Jacobian

$$\mathbf{J}^{-1} = \begin{pmatrix} \frac{\partial p_1}{\partial q_1} & \frac{\partial p_1}{\partial q_2} & \dots & \frac{\partial p_1}{\partial q_N} \\ \dots & \dots & \dots & \dots \\ \frac{\partial p_N}{\partial q_1} & \frac{\partial p_N}{\partial q_2} & \dots & \frac{\partial p_N}{\partial q_N} \end{pmatrix} . \quad (2.7)$$

The form of the mapping \mathbf{v} is determined by the choice of filters in equation 2.5. These in turn are chosen to ensure that the determinant of the Jacobian is everywhere non-zero and also to minimise the sum (over all parameter space) of errors in the parameter space vectors \mathbf{p} which are introduced by experimental errors and projected through the inversion process back into parameter space.

Two sources of error were highlighted by Preece & Claridge both of which can be expressed as errors in the image values c_l (equation 2.4). The first is an assumed constant error in each c_l introduced by the camera and the second is an error in each reflectance spectrum calculation (equation 2.3) which is passed on to the c_l values through equation 2.4. Thus, we have an error associated with the l 'th image value and with the parameter space location \mathbf{p} which is the outcome of two independent errors

$$\sigma_{c_l}(\mathbf{p}) = \sqrt{\sigma_{c_l,C}^2(\mathbf{p}) + \sigma_{c_l,S}^2(\mathbf{p})} \quad (2.8)$$

where $\sigma_{c_l,C}(\mathbf{p})$ is the constant camera error

$$\sigma_{c_l,C}(\mathbf{p}) = \sigma_C$$

and $\sigma_{c_l,S}(\mathbf{p})$ is the error introduced by the body reflectance spectral error ($\sigma_s(\lambda)$) at wavelength λ

$$\sigma_{c_l,S}(\mathbf{p}) = \sqrt{\int (\sigma_S(\lambda) F_l(\lambda))^2 d\lambda} . \quad (2.9)$$

Using $\sigma_{c_l}(\mathbf{p})$ we can derive the error in every parameter value p_n at all points in parameter space

$$\sigma_{p_n}(\mathbf{p}) = \sqrt{\sum_{l=1}^{N+1} \left(\frac{\partial p_n}{\partial c_l}\right)^2 \sigma_{c_l}^2(\mathbf{p})} \quad .$$

Noting that

$$\frac{\partial p_n}{\partial c_l} = \frac{1}{c_1} \frac{\partial p_n}{\partial q_{l-1}} \quad l = 2, \dots, N+1$$

and

$$\frac{\partial p_n}{\partial c_1} = -\frac{1}{c_1} \sum_{l=1}^N q_l \frac{\partial p_n}{\partial q_l}$$

$$\sigma_{p_n}(\mathbf{p}) = \frac{1}{c_1} \sqrt{\sigma_{c_1}^2(\mathbf{p}) \left(\sum_{l=1}^N \frac{\partial p_n}{\partial q_l} q_l\right)^2 + \sum_{l=1}^N \sigma_{c_{l+1}}^2(\mathbf{p}) \left(\frac{\partial p_n}{\partial q_l}\right)^2} \quad (2.10)$$

with the partial derivatives obtained from \mathbf{J}^{-1} (equation 2.7) evaluated at each point \mathbf{p} in parameter space.

2.3 The N+1 filter model when N=1

In comparing the technique with alternatives we will consider the simplest case of a one dimensional parameter space and two filters ($F_1(\lambda)$ and $F_2(\lambda)$). Thus we have one parameter p and the mapping of the parameter space consists of setting a linearly spaced range of values of p from p_{min} to p_{max} . For each value of p we evaluate a reflectance spectrum $I_r(\lambda)$ by modelling the transport of light in the material. Using the set of spectra and assuming there is Gaussian noise on the spectral data ($\sigma_s(\lambda)$ in equation 2.9) we then construct the mapping $p \rightarrow q$ given by

$$q(p) = \frac{\int I_r(\lambda) F_2(\lambda) d\lambda}{\int I_r(\lambda) F_1(\lambda) d\lambda}$$

(the p dependence emerging through $I_r(\lambda)$). Our Jacobian reduces to $\frac{\partial q}{\partial p}$ and its inverse to $\frac{\partial p}{\partial q}$ yielding a parameter error (equation 2.10)

$$\sigma(p) = \frac{1}{c_1} \frac{\partial p}{\partial q} \sqrt{q^2 \sigma_{c_1}^2(p) + \sigma_{c_2}^2(p)} \quad . \quad (2.11)$$

It is the errors $\sigma(p)$ $p_{min} < p < p_{max}$ that we minimize by using an optimisation technique to select $F_1(\lambda)$ and $F_2(\lambda)$.

Chapter 3

Linear Multivariate Techniques

When dealing with the highly correlated information associated with spectra it is common practice to apply linear multivariate analysis methods which replace the large number of independent variables (the wavelength dependent spectral values) with a few latent variables (each of which is a linear combination of the original variables) on which regression is performed. The method of choosing the latent variables defines different techniques and the most commonly known are principal component regression (PCR) and partial least squares (PLS). More recently these have been shown to be a subset of principal covariates regression [9] (a continuum regression technique[10] in which the value of an adjustable parameter determines how the latent variables are constructed). These methods of inverting spectral data are broadly used and have been applied to studies on skin cancer[11], the ripeness of tomatoes[12], contaminants in groundwater[13][14], the classification of wheat[15], fungus in corn[16], pulp yields in paper production[17] and many others (see the review articles by Thomas [18] and Brown et. al. [19] for further examples). Given a sample set of spectra with known values for the dependent variable these methods use linear modelling (or soft modelling[20]) to approximate the relations in the data. These linear approximations are developed about a typical sample value and for this reason the dependent and independent variables need to be centred by subtracting the mean at each wavelength from the spectral values and the mean of the dependent variable values from the dependent variable values.

By using the NIPALS algorithm[21] for PCR we extract the principal components in such a way that the component representing the maximum spread on our centred spectra is removed first. Similarly in PLS we use orthogonalised partial least squares regression[22] to extract scores such that the maximum covariance between the remaining centred spectral data and the remaining centred dependent data is represented at each iteration. Deciding

how many latent variables to extract in either case determines the size of the soft model and is the most critical step in the process and remains more art than science[20]. If too few latent variables are used then the linear model will insufficiently represent the complexity of the relationship between the dependent and independent variables whereas redundant latent variables may be attempting to model noise in the sample data. We can avoid this problem because our hard model of the interaction of light and matter will produce both the sample spectra from which we build the regression models and the test spectra with which we compare the techniques. The sample spectra will have no noise associated with them, so that we can take arbitrarily many latent variables until the remaining centred data has insignificant variance (say 10^{-20} of that associated with the first component/score). As we evaluate the errors obtained when attempting to invert the test spectra we shall simply choose the number of latent variables which yields the lowest error on the reconstructed dependent variable.

Chapter 4

Experimental method

4.1 The one-dimensional problem

Using the method described in chapter 2 we define a one dimensional problem which allows us to compare the ability of this technique with those of linear multivariate methods to reconstruct the parameter value given multivariate data (in the form of spectra). Consider the setup in figure 4.1. An infinite homogenous layer of turbid material (material 2) lies beneath a thin layer of a similar light scattering material (material 1) and diffuse light incident on the top layer will either be absorbed in one of the materials or be scattered and finally emerge to contribute to the reflectance spectrum. As the thickness of material 1 is changed the reflectance spectrum will vary from that of material 2 only (when the layer thickness is nil) to that of material 1 only (when the thickness is so great that no light penetrates to layer 2).

The parameters that will determine the spectra at the two extreme cases are the macroscopic scattering and absorption cross sections in each material ($\Sigma_{s,1}(\lambda), \Sigma_{s,2}(\lambda), \Sigma_{a,1}(\lambda), \Sigma_{a,2}(\lambda)$). The choice of these parameters is governed by the need to represent realistic physical quantities while keeping the wavelength dependence as simple as possible. Thus scattering is assumed to decrease inversely with the fourth power of the wavelength (in accordance with Rayleigh scattering) with maximum values large compared to the absorption cross sections to ensure a reasonable reflectance from each material. The scattering cross sections are depicted in figure 4.2.

Absorption cross sections were given a more flexible Gaussian variation with wavelength. We have considered four different cases: a) where the two absorption cross sections have equal maxima and are well separated with means at 400 nm and 700 nm and each with a standard deviation of 80 nm ; b) where the two Gaussians are as in a) except that their overlap is much greater with

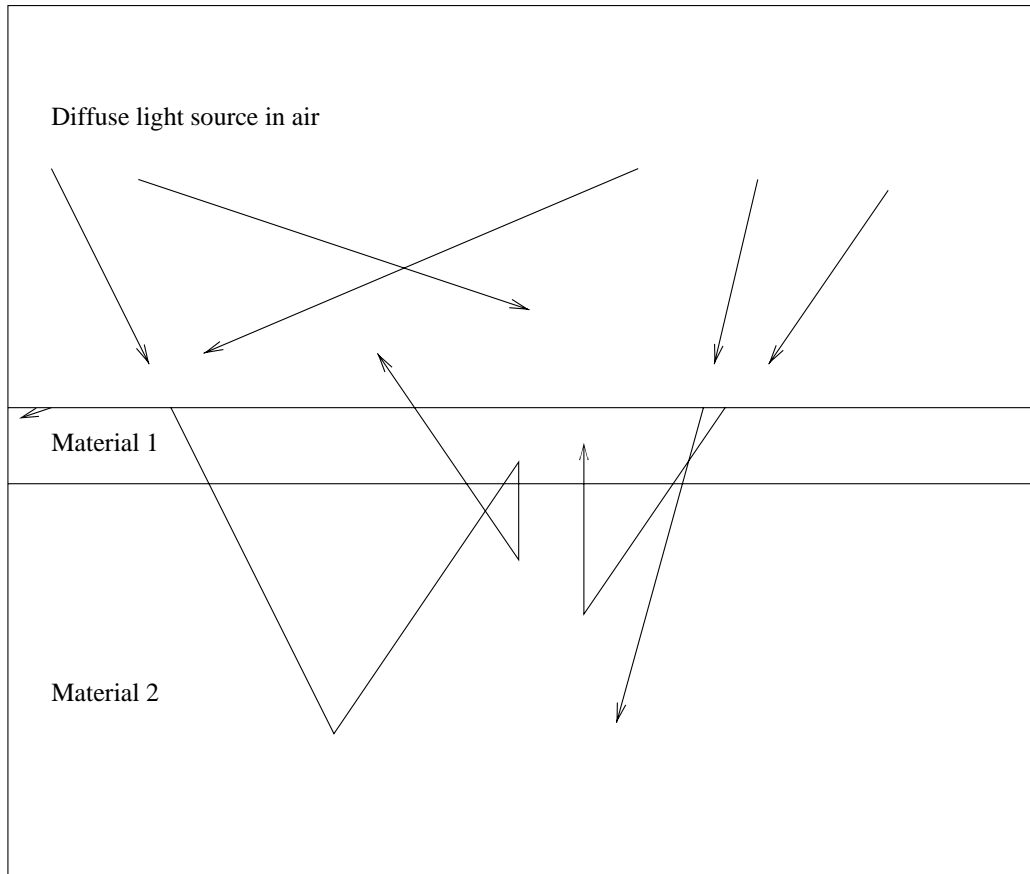


Figure 4.1: Light being absorbed and scattered by a thin layer of material 1 lying on an infinite layer of material 2.

the separation of their means being equal to their common standard deviation (80 nm); c) in which the absorption cross section of material 2 has been reduced and broadened (maximum reduced to half that of material 1 and standard deviation increased to 240 nm) with the means separated by 100 nm ; d) with absorption cross sections as in c) except that they have equal means. The absorption cross sections for the four cases are depicted in figure 4.3.

The range of thicknesses of the top layer was chosen so that at a maximum of 15 microns it made the probability of a scatter in the top layer very likely ($\Sigma_{s,1}(\lambda = 300\text{ nm}) = 1\mu^{-1}$).

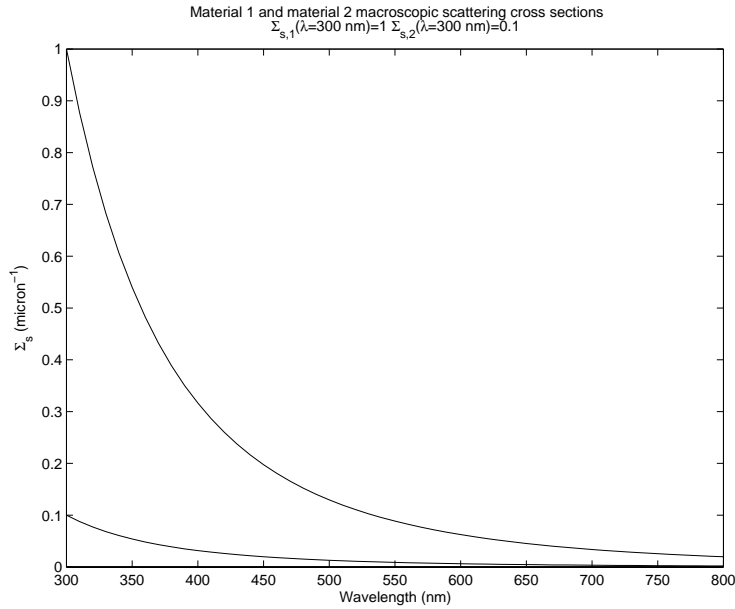


Figure 4.2: Macroscopic scattering cross sections in the foreground (1) and background (2) materials.

4.2 The sample reflectance spectra

Using our cross section data we can evaluate the reflectance spectrum for a given thickness of layer 1 from the Kubelka-Munk model [23] (see [24]). Although based on a simple energy flow balance this model yields reflectance and (in the case of finite thickness layers) transmittance formulae which were identified by Klier [25] as identical to the solution of the radiative transfer equation (single energy transport equation [26]) when simplified to deal with infinite area, homogeneous, intensely isotropically scattering layers [27].

We start with a thickness of zero (producing the reflectance spectrum of material 2) and the four cases are shown in figure 4.4. These spectra are independent of material 1 and show a high reflectance over the wavelength range of the visible spectrum (due to the very large ratio scatter/absorption in material 2) with a dip near the peak in the absorption cross section but with its minimum shifted to higher wavelengths due to the corresponding fall in $\Sigma_{s,2}(\lambda)$. In the task of analysing the final output spectra obtained as we add different thicknesses of layer 1 to layer 2 we can think of this as our “base” spectrum onto which the increasing influence of the scattering and absorption characteristics of material 1 is added until layer 1 is thick enough to prevent transmission of light to layer 2. At that point we have the spectra

shown in figure 4.5.

Increasing the thickness of layer 1 will have no further effect on these spectra and they are independent of material 2. It is the transformation from the “base” spectra in figure 4.4 to those in figure 4.5 (which we refer to as “the layer 1 saturation spectra”) as we increase the thickness of layer 1 which must be analysed in order to differentiate a given layer 1 thickness. The four sets of spectra shown in figure 4.6 show the change in response as the thickness of layer 1 is varied linearly from 0 to 15μ . This is a subset of our sample spectra (there are 100 spectra in the full set) which we use to generate optimal filters (in SFO), principal components and loadings (in PCR) and scores and loadings (in PLS).

4.3 Results

In order to compare the three techniques we next generate a set of 100 test spectra in which the thickness of layer 1 ($y'_i, i = 1, 100$) is randomly chosen to lie in the same range (0 to 15μ) as those of the sample spectra. We then invert the spectra using the optimal filters from SFO to obtain $y'_{O,i}, i = 1, 100$ and the regression results from the linear multivariate methods PCR (to obtain $y'_{R,i}, i = 1, 100$) and PLS (to give $y'_{S,i}, i = 1, 100$). As error measures we use the root mean sum of squares

$$RMSOS_{O/R/S} = \sqrt{\frac{\sum_{i=1}^{100} (y'_i - y'_{O/R/S,i})^2}{100}}$$

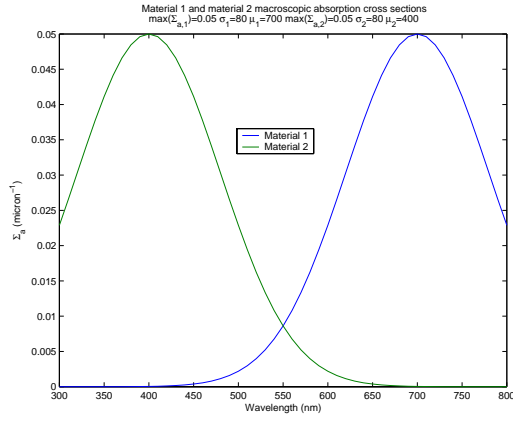
and the mean absolute percentage error

$$MAPE_{O/R/S} = \sum_{i=1}^{100} \frac{abs(y'_i - y'_{O/R/S,i})}{y'_i}.$$

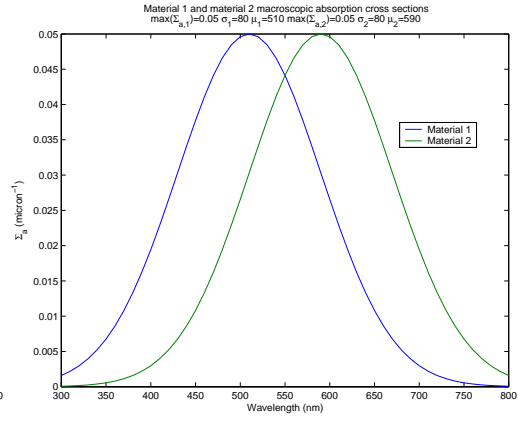
As stated in chapter 3 we choose the number of latent variables in PCR and PLS which yield the minimum error measure in each case. Not surprisingly the three methods yield excellent results (since the same hard model was used to generate both sample and test spectra) with, for instance, RMSOS values of $7.5 \times 10^{-4}\mu$ for SFO, $2 \times 10^{-3}\mu$ for PCR (with 9 or more latent variables) and $2 \times 10^{-8}\mu$ for PLS (with 17 latent variables). To simulate the effect introduced when dealing with real data we then add Gaussian noise with a fixed standard deviation to our test spectra before inverting them to calculate RMSOS and MAPE values. The process is repeated with increased standard deviation up to a maximum of 2×10^{-2} in steps of 2×10^{-4} (our

test spectral values lie between 0.1 and 1). In figure 4.7 we show a selection of the test data used in case a) with no added noise and then with added Gaussian noise of standard deviations 0.001, 0.01 and 0.02.

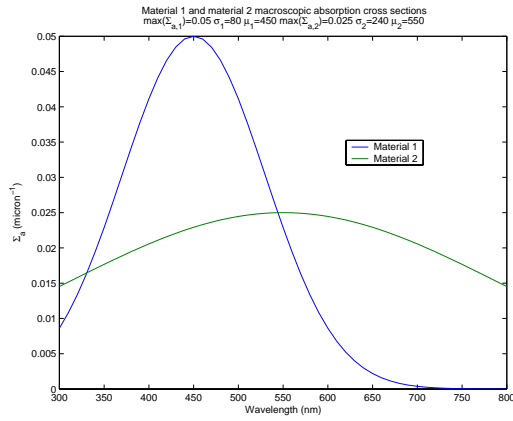
The results are shown in figures 4.8 (RMSOS) and 4.9 (MAPE). As might be expected the errors in all three techniques increase with the size of the added noise. The influence of changing the method of linear multivariate regression is insignificant when compared with the reduction in errors achieved with SFO. To emphasize the difficulties encountered by linear multivariate inversion when noise is added to the test data we plot the optimal number of latent variables chosen (to yield the minimum errors plotted in figure 4.8) in figure 4.10. Whereas, with no noise, many latent variables (typically 9 for PCR and 17 for PLS) yield the optimum results, with increasing noise, the fine tuning obtained with higher order soft models rapidly becomes a source of increased error.



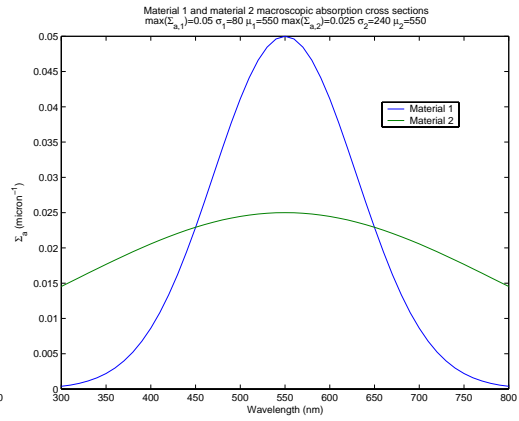
(a)



(b)

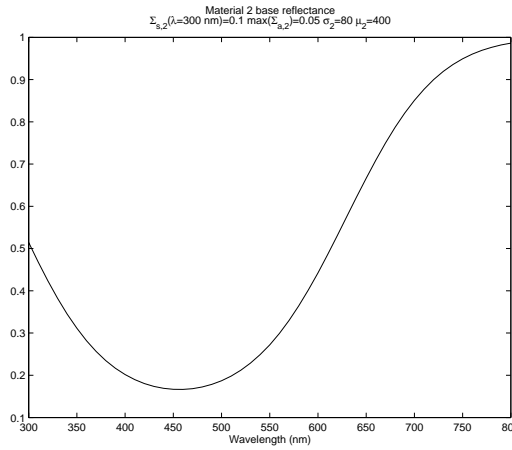


(c)

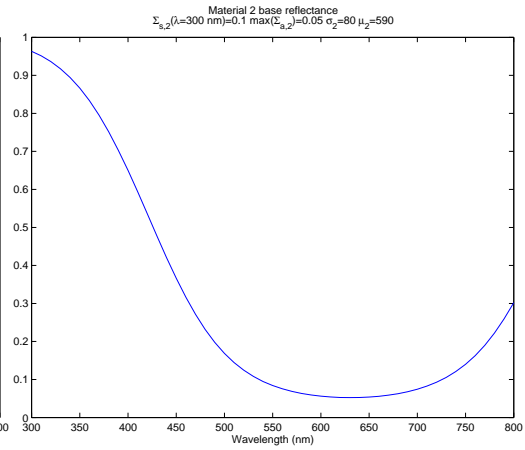


(d)

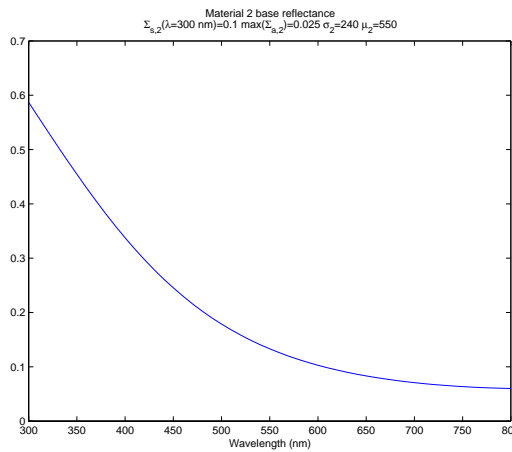
Figure 4.3: Macroscopic absorption cross sections in the foreground (1) and background (2) materials which determine our 4 cases a),b),c) and d).



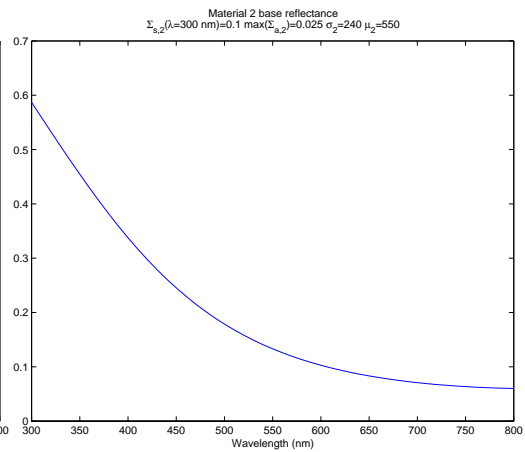
(a)



(b)

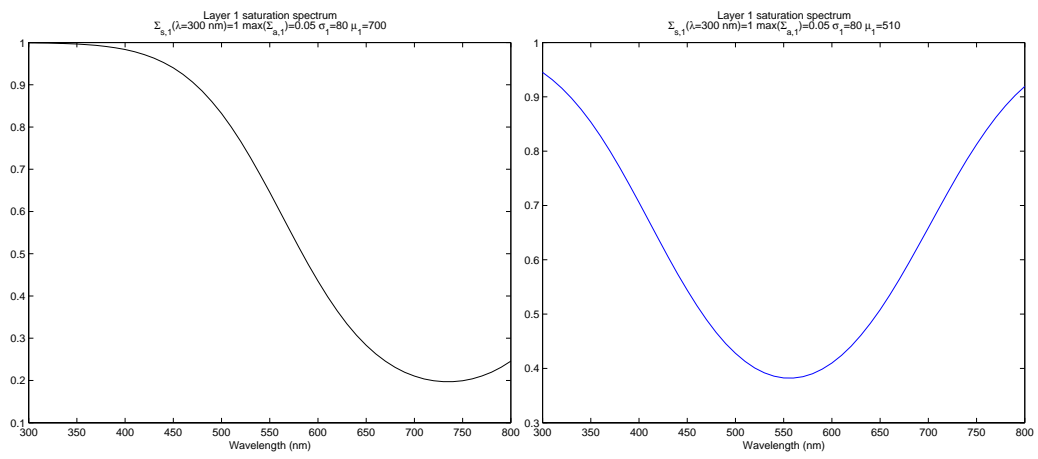


(c)



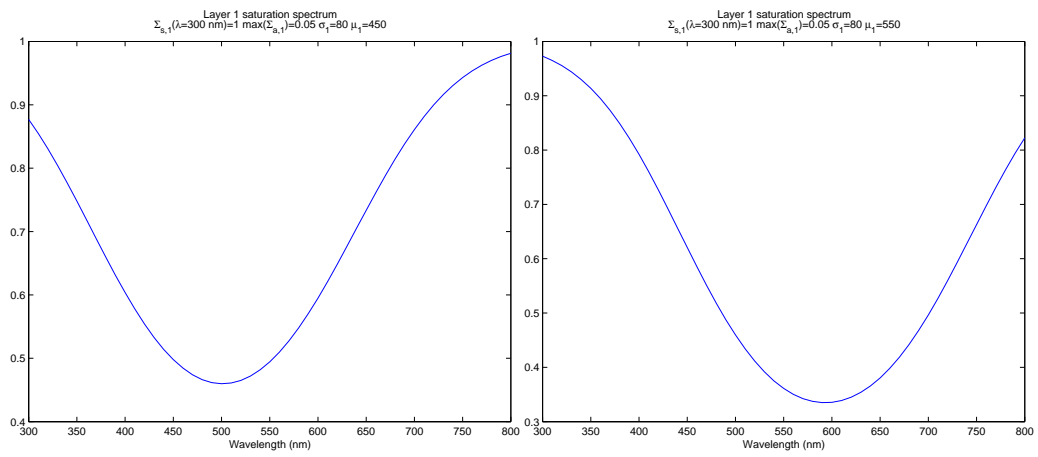
(d)

Figure 4.4: Base reflectance spectrum of material 2 in our 4 cases (see figure 4.3).



(a)

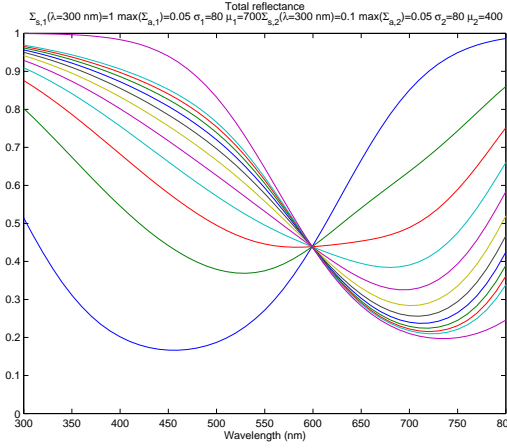
(b)



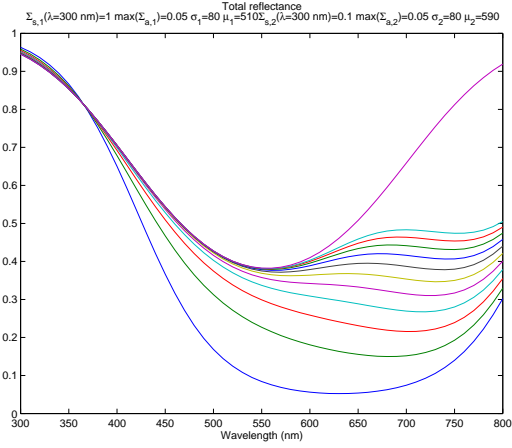
(c)

(d)

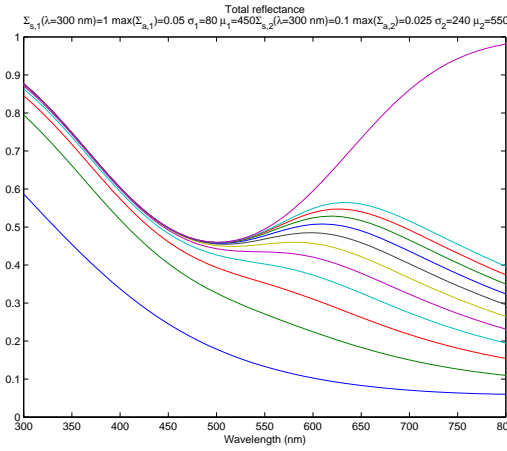
Figure 4.5: Layer 1 saturated spectrum in each of the 4 cases (see figure 4.3).



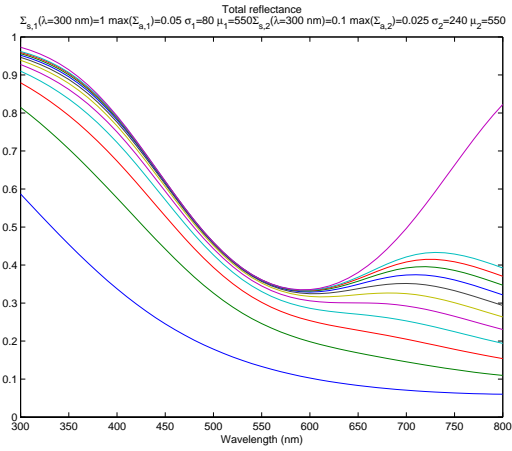
(a)



(b)



(c)



(d)

Figure 4.6: Range of spectra as layer 1 $d = 0 \rightarrow 15\mu$ in the 4 cases (see figure 4.3).

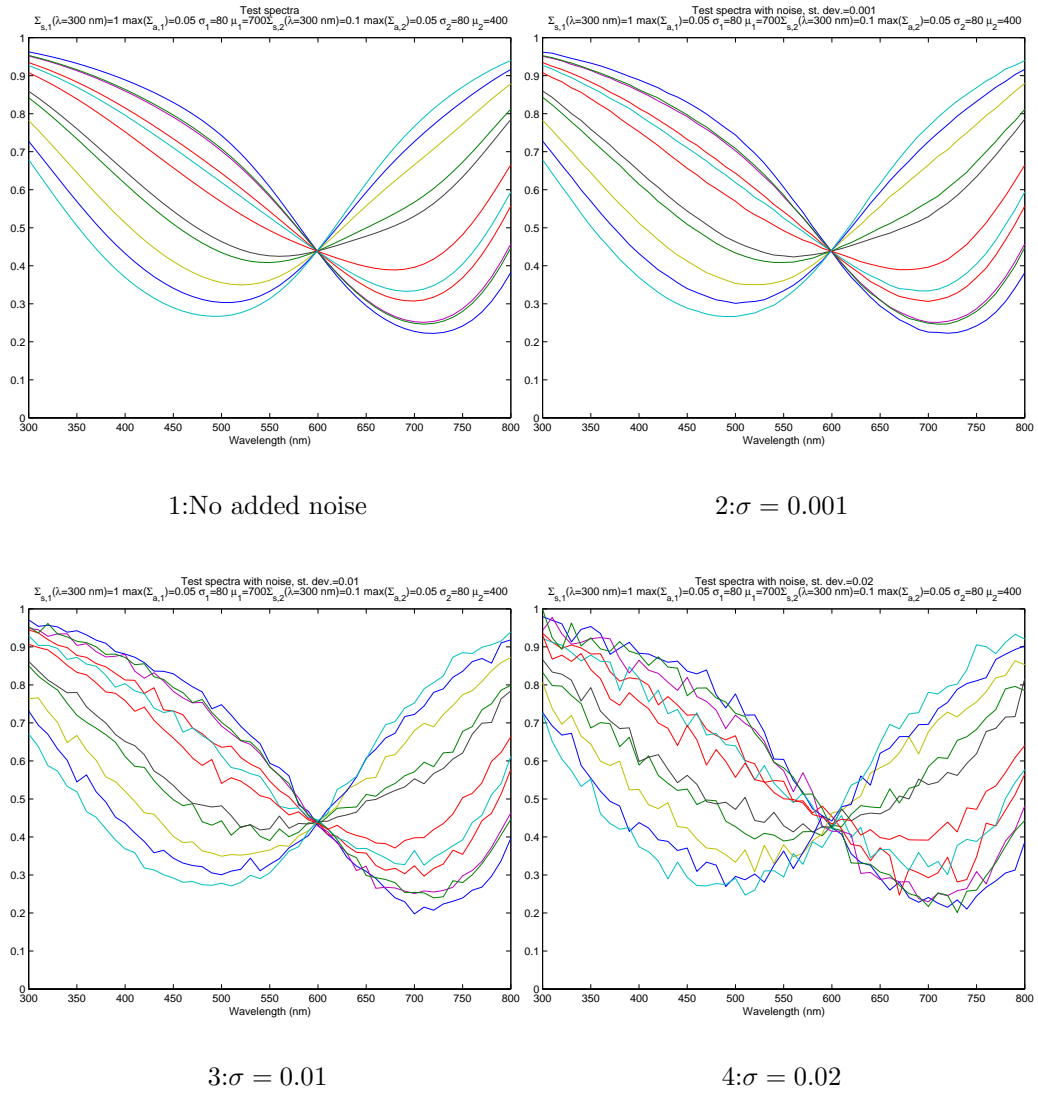
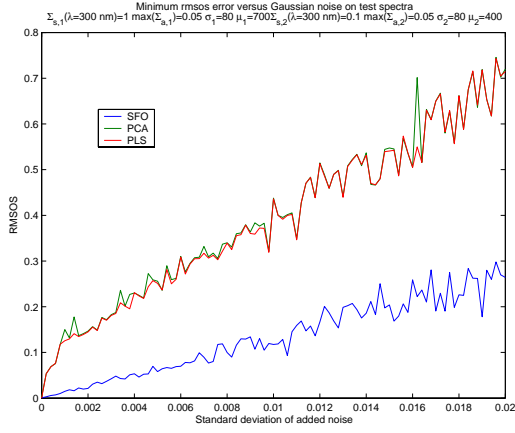
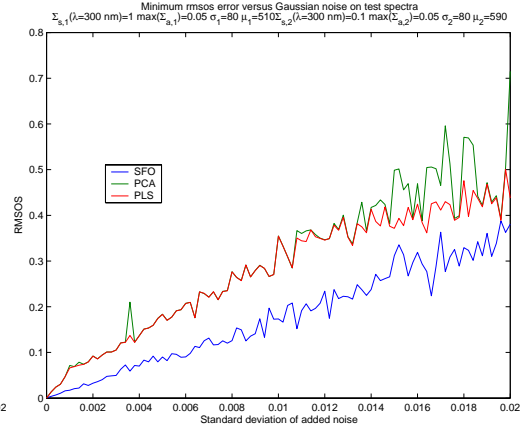


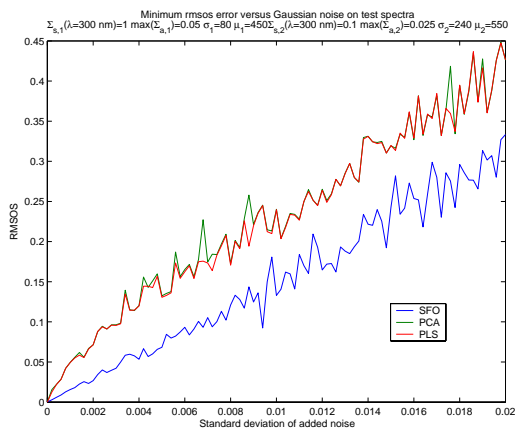
Figure 4.7: Sample test data with added Gaussian noise covering the range of standard deviation in figures 4.8,4.9 and 4.10.



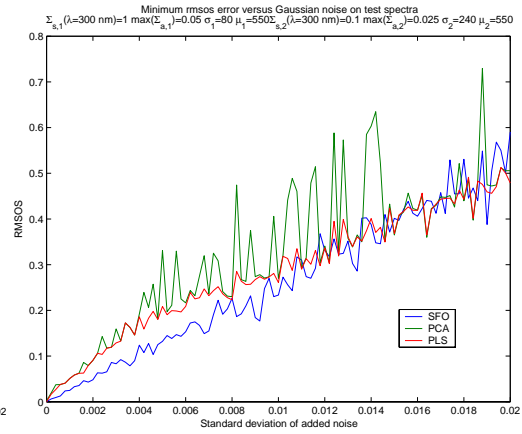
(a)



(b)

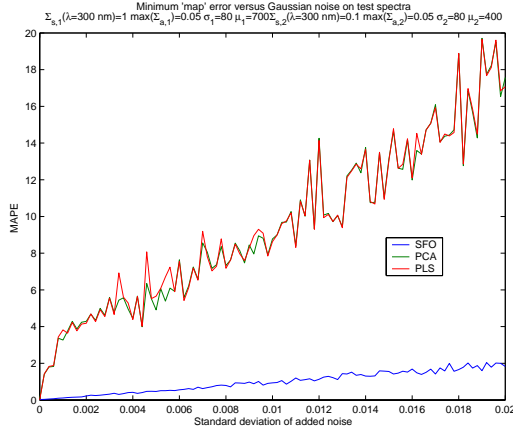


(c)

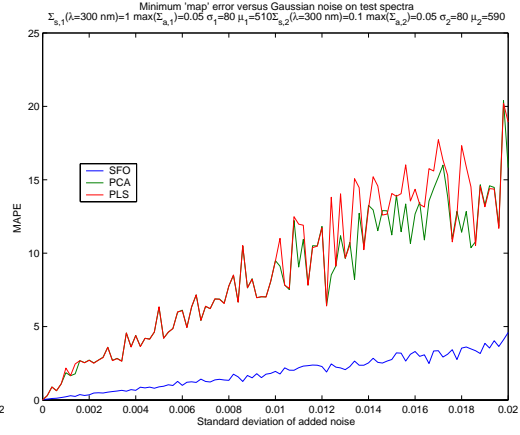


(d)

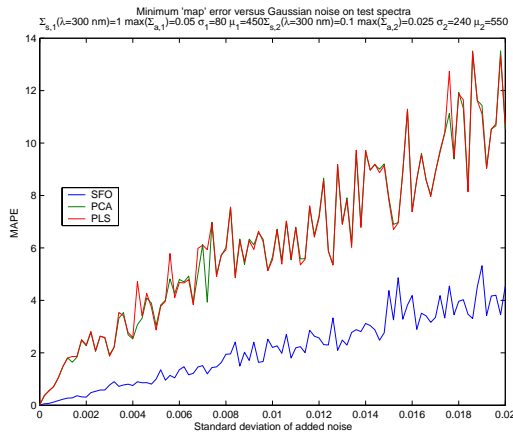
Figure 4.8: Comparing the RMSOS errors in SFO, PCR and PLS as a function of the standard deviation of Gaussian noise added to test data in our 4 cases (see figure 4.3).



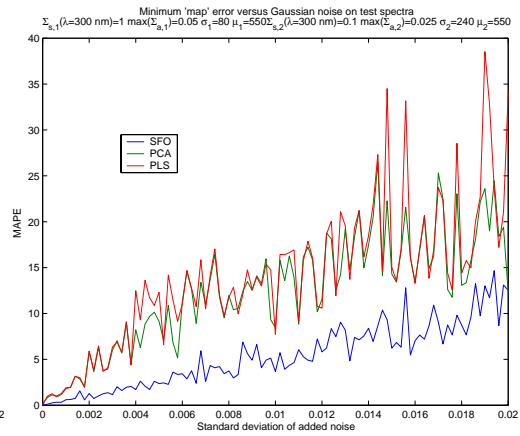
(a)



(b)

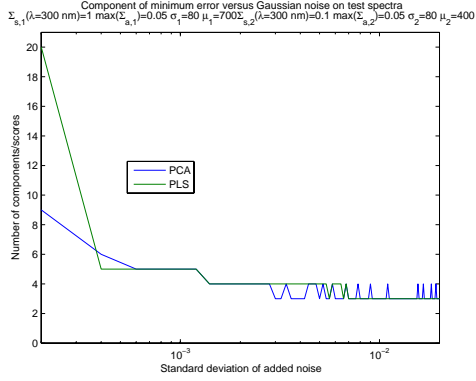


(c)

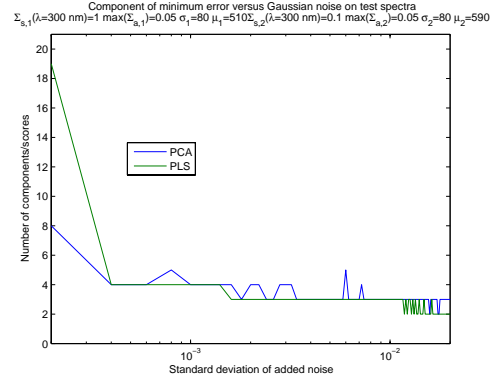


(d)

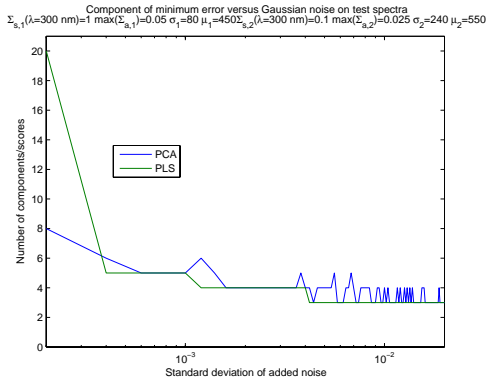
Figure 4.9: Comparing the MAPE in SFO, PCR and PLS as a function of the standard deviation of Gaussian noise added to test data in our 4 cases (see figure 4.3).



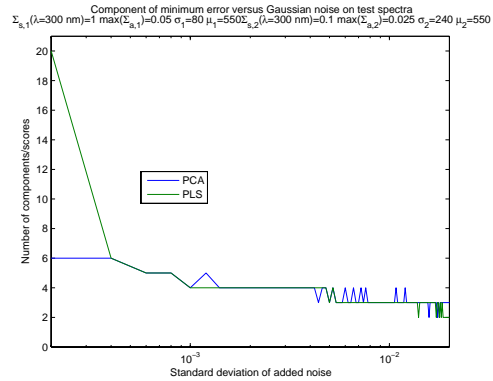
(a)



(b)



(c)



(d)

Figure 4.10: Number of components/scores used to obtain minimum RM-SOS errors in PCR/PLS inversion of test spectra as a function of standard deviation of added Gaussian noise in our 4 cases (see figure 4.3). (Note the logarithmic x-axis to enhance the display. The x-axis origin corresponds to no added noise).

Chapter 5

Discussion

The broad swathe of applications of linear multivariate analysis make it a powerful diagnostic which is continually being refined [19]. Its main advantage is its ability to build linear models which describe the relationship between many dependent variables and many independent variables by considering the statistical correlation between the variables without any need to understand the physical processes involved in those relationships.

By comparison SFO must know a priori the total number of independent variables (N). This enables it to create a nonlinear mapping to N ratio values constructed from $N+1$ filters. In order to build the nonlinear mapping SFO requires sample spectra covering the entire N dimensional parameter space so as to construct an accurate approximation to the Jacobian at any point. These two requirements, although not necessitating it, are most easily met when a theoretical model exists linking the unknown (dependent) variables with the multivariate data (spectra).

The chief advantage of SFO is its automatic inclusion of realistic physical errors into the filter construction process. Its minimization of the error propagation from source (camera, spectrum, etc.) through to the dependent variable evaluation ensures the technique focusses on accurate parameter recovery.

Acknowledgements

This work was supported by the Leverhulme Trust Grant No. F/00 094/M.

Bibliography

- [1] S. Preece and E. Claridge, “Spectral filter optimisation for the recovery of parameters which describe human skin,” *IEEE Trans. Patt. Anal. and Mach. Int.*, vol. 26, no. 7, pp. 913–922, 2004.
- [2] K. Faber and B. R. Kowalski, “Propogation of measurement errors for the validation of predictions obtained by principal component regression and partial least squares,” *J. Chemometrics*, vol. 11, pp. 181–238, 1997.
- [3] S. A. Shafer, “Using color to separate reflection components,” *Color Research and Application*, vol. 10, pp. 210–218, Winter 1985.
- [4] S. Tominaga and B. A. Wandell, “Standard surface-reflectance model and illuminant estimation,” *J. Opt. Soc. Am. A*, vol. 6, pp. 576–584, April 1989.
- [5] G. Healey, “Using color for geometry-insensitive segmentation,” *J. Opt. Soc. Am. A*, vol. 6, pp. 920–937, June 1989.
- [6] H.-C. Lee, “Method for computing the scene-illuminant chromaticity from specular highlights,” *J. Opt. Soc. Am. A*, vol. 3, pp. 1694–1699, October 1986.
- [7] S. Tominaga and B. A. Wandell, “Component estimation of surface spectral reflectance,” *J. Opt. Soc. Am. A*, vol. 7, pp. 312–317, February 1990.
- [8] S. Preece and E. Claridge, “A technique for geometry-insensitive recovery of quantitative scene parameters from images,” Tech. Rep. CSR-04-08, School of Computer Science, The University of Birmingham, 2004.
- [9] S. deJong and H. Kiers, “Principal covariates regression: Part 1, theory,” *Chemom. Intel. Lab. Syst.*, vol. 14, pp. 155–164, 1992.
- [10] M. Stone and R. J. Brooks, “Continuum regression: Cross-validated sequentially constructed prediction embracing ordinary least squares,

- partial least squares and principal component regression,” *J. R. Statist. Soc. B*, vol. 52, pp. 237–258, 1990.
- [11] V. P. Wallace, J. C. Bamber, D. C. Crawford, R. J. Ott, and P. S. Mortimer, “Classification of reflectance spectra from pigmented skin lesions, a comparison of multivariate discriminant analysis and artificial neural networks,” *Phys. Med. Biol.*, vol. 45, pp. 2859–2871, 2000.
- [12] G. Polder, G. W. A. M. van der Heijden, and I. T. Young, “Hyperspectral image analysis for measuring ripeness of tomatoes.” Presented at the 2000 ASAE International meeting, Paper No. 003089 ASAE, 2950 Niles Road, St. Joseph. MI 49085-9659 USA., July 2000.
- [13] T. G. Diaz, A. Guiberteau, J. M. O. Burguillos, and F. Salinas, “Comparison of chemometric methods: Derivative ratio spectra and multivariate methods (cls, pcr and pls) for the resolution of ternary mixtures of the pesticides carbofuran carbaryl and phenamifos after their extraction into chloroform,” *Analyst*, vol. 122, pp. 513–517, 1997.
- [14] R. C. Tena, M. A. R. Delgado, M. J. Sanchez, and F. G. Montelongo, “Comparative study of the zero-crossing, ratio spectra derivative and partial least squares methods applied to the simultaneous determination of atrazine and its degradation product desethylatrazin-2-hydroxy in ground waters,” *Talanta*, vol. 44, pp. 673–683, 1997.
- [15] D. Wang, F. E. Dowell, and R. E. Lacey, “Single wheat kernel size effects on near-infrared reflectance spectra and color classification,” *Cereal Chem.*, vol. 76, no. 1, pp. 34–37, 1999.
- [16] F. E. Dowell, T. C. Pearson, E. B. Maghirang, F. Xie, and D. T. Wicklow, “Reflectance and transmittance spectroscopy applied to detecting fumonisin in single corn kernels infected with fusarium verticillioides,” *Cereal Chem.*, vol. 79, no. 2, pp. 222–226, 2002.
- [17] N. L. Sefara, D. Conradie, and P. Turner, “Progress in the use of near-infrared spectroscopy as a tool for the rapid determination of pulp yield in plantation eucalypts,” *TAPPSA Journal*, pp. 15–17, November 2000.
- [18] E. V. Thomas, “A primer on multivariate calibration,” *Anal. chem.*, vol. 66, no. 15, pp. 795A–804A, 1994.
- [19] S. D. Brown, S. T. Sum, F. Despagne, and B. K. Lavine, “Chemometrics: Fundamental review,” *Anal. chem.*, vol. 66, pp. 21R–61R, 1996.

- [20] S. D. Brown, "Information and data handling in chemistry and chemical engineering: the state of the field from the perspective of chemometrics," *Comp. Chem. Engng.*, vol. 23, pp. 203–216, 1998.
- [21] H. Wold, "Estimation of principal components and related models by iterative least squares," in *Multivariate Analysis* (P. Krishnaiah, ed.), pp. 391–420, New York: Academic Press, 1966. Proceedings of an International Symposium held in Dayton, Ohio, June 14-19, 1965.
- [22] H. Martens and T. Naes, *Multivariate Calibration*. John Wiley and Sons Ltd., 1960.
- [23] P. Kubelka and F. Munk, "Ein beitrag zur optik farbanstriche," *Z. fur Tech. Phys.*, vol. 12, pp. 593–601, 1931.
- [24] F. Steele, "The optical characteristics of paper," *Paper Trade Journal. Technical Association Section.*, pp. 151 –156, March 1935.
- [25] K. Klier, "Absorption and scattering in plane parallel turbid media," *J. Opt. Soc. Am.*, vol. 62, pp. 882–885, July 1972.
- [26] G.I.Bell and S. Glasstone, *Nuclear Reactor Theory*, ch. 2, p. 65. New York: Van Nostrand Reinhold Company, 1970.
- [27] S. Chandrasekhar, *Radiative Transfer*. New York: Dover Publications, Inc., 1960.